

Deep Representations for Iris, Face, and Fingerprint Spoofing Attack Detection

David Menotti[✉], *Member, IEEE*, Giovani Chiachia[✉], Allan Pinto, *Student Member, IEEE*,
William Robson Schwartz, *Member, IEEE*, Helio Pedrini, *Member, IEEE*,
Alexandre Xavier Falcão, *Member, IEEE*, and Anderson Rocha, *Member, IEEE*

Abstract—Biometrics systems have drastically improved person identification and/or authentication, playing an important role in personal, national, and global security. However, such systems might be deceived or “spoofed” and, despite the advances in spoofing detection to each biometric modality, there is still a lack of a clearly unified approach. Aiming at filling this gap, we propose a unified framework to learn deep representations for three different modalities of spoofing biometrics (i.e., face, iris, and fingerprint). The representations are learned directly from the data with an optimization procedure that randomly searches for the best convolutional neural network from a family of networks defined in a hyperparameter search space. Atop these representations, we couple a linear Support Vector Machine classifiers for the final decision making. Instead of learning thousands and/or millions of network weights/parameters based either on backpropagation-like or unsupervised feature learning techniques, our networks use random filter weights initialized in a convenient way, which allows us to quickly probe thousands of network configurations. Experiments on nine publicly available benchmarks of these three modalities show that our framework achieves either very competitive or state-of-the-art results for all problems and modalities.

Index Terms—Deep Representation Learning, Convolutional Neural Networks, Hyperparameter Optimization, Spoofing Attack Detection.

I. INTRODUCTION

B IOMETRICS human characteristics and traits can successfully allow people identification and authentication and have been widely used for access control, surveillance, and also in national and global security systems [1]. In the last few years, due to the recent technological improvements for data acquisition, storage and processing, and also the scientific advances in computer vision, pattern recognition, and machine learning areas, several biometric modalities have been largely applied to person recognition ranging from the traditional fingerprint one to face, to iris, and more recently to vein and blood flow identification. Simultaneously, various *spoofing attack* techniques have been created to defeat the biometric

systems. Therefore, the security of such systems against the myriad possible attacks is still an open problem [2].

There are several ways to attack a biometric system [3], [4]. In the literature, we can find a study analyzing eight different points of attack on biometric systems [5], [6]. These attacks can be divided into two main groups: *direct* and *indirect* attacks. The former, the focus of this work, considers the possibility to generate synthetic biometric samples and is the first vulnerability point of a biometric security system acting in the sensor level. The latter includes all the remaining seven points of attacks and requires different levels of knowledge of the system, e.g., the matching algorithm used, the specific feature extraction procedure, database access for manipulation, and also possible weak links in the communication channels within the system.

Given that the most vulnerable part of a system is its acquisition sensor, the attackers have mainly focused on direct spoofing attacks. To complicate, several biometric traits can be easily acquired by other devices serving as input for the real biometric systems (e.g., faces, iris, fingerprint, and voice). Although the definition of liveness detection (aka spoofing attack) is clear¹, most of the existing solutions in the literature address the spoofing detection by presenting solutions custom-tailored for specific modalities.

In the context of face modality, impostors can perform a spoofing attack to a biometric system by presenting to the acquisition sensor a photography, a digital video or even a 3D facial model (mask) of a valid user. In the iris modality, the spoofing attack take place using printed iris spoof images [8] or even more interesting (although much more expensive), it can use cosmetic contact lenses. In the latter case, the spoofing detection task is normally focused on the obfuscation of the iris texture due to the use of lenses rather than on the image telltales [9], [10]. Finally, considering the fingerprint modality, the most common attack consists of using an artificial replica [11] created in a cooperative way. A mold of the negative fingerprint is acquired with the subject cooperation from which a replica is built or filled with different materials including gelatin, latex, play-doh or silicone. Latent fingerprints left on a surface may also be used and further enhanced after acquisition with a digital camera. Then the negative fingerprint can be printed on a transparent sheet and used to attack a specific system.

¹Determining if the biometric being captured is an actual measurement from the authorized, live person who is present at the time of capture [7].

D. Menotti, G. Chiachia, A. Pinto, H. Pedrini, A. Rocha and A. X. Falcão are with the Institute of Computing, University of Campinas, Campinas, SP, 13083-852, Brazil. email: menottid@gmail.com, {chiachia,allan.pinto,helio.pedrini,anderson.rocha,afalcao}@ic.unicamp.br.

W. R. Schwartz is with the Computer Science Department, Federal University of Minas Gerais, Belo Horizonte, MG, 31270-010, Brazil. email: william@dcc.ufmg.br.

D. Menotti is also with Computing Department, Federal University of Ouro Preto, Ouro Preto, MG, 35400-000, Brazil (he has spent his sabbatical year (2013-2014) at IC-UNICAMP). email: menotti@iceb.ufop.br.

✉ These authors contributed equally to this work.

Manuscript received October 1st, 2014;.

As previously mentioned, until now, the success of an anti-spoofing system was directly connected to the modality for which it was designed. Normally, such systems include expert knowledge and a substantial effort on feature engineering processes to properly capture acquisition telltales left by the different types of attacks. However, the need of custom-tailored solutions for the myriad possible attacks is a very limiting constraint as small changes in the attack could mean entire system redesign needs. Therefore, in this paper, we present a unified framework to learn deep representations for different biometric spoofing modalities: fingerprints, faces, and irises – the three most used nowadays.

We deal with the spoofing attack problem related to these three types of modalities that were targeted in recent biometrics competitions, i.e., face [12], [13], iris [14], [8], and fingerprint [7], [15], [11]. The unified framework we propose herein learns deep representations [16] for different biometric spoofing modalities. These representations are biologically inspired and have been successfully used in the face recognition context [17], [18], [19] by our team. It also has been recently employed by our team for handheld printed iris spoofing attacks with promising results [8].

Deep learning (DL) techniques have shown a great success in several computer vision tasks with groundbreaking results [20], [21], [22], [23], [24] for many difficult problems. Allied with their success, DL techniques enable us to learn multi-layered (hence the term deep) representations directly from the data. This powerful representation allows us to find deep representational connections that would be hardly thought by a human expert.

The learned representations model the distribution of real and fake classes yielding outstanding liveness detection methods [8]. Here, we are particularly interested in the use of a specific type of technique for learn deep representations: the convolutional neural networks (CNN), which was initially introduced by LeCun *et al.* [25].

Instead of using either a backpropagation-like algorithm to learn the network weights of a CNN with a predefined topology such as done in other works [26], [21], [24] or estimating the weights using an unsupervised learning algorithm [27], [28], [29], we opt to optimize the network architecture and its hyper-parameter space. On the top of these learned representations, we attach a discriminative classifier, the Support Vector Machines (SVMs) with linear kernels and hard margins [30], [31]. It is worth mentioning that other classifiers could be considered here as well. In the architecture optimization, we study and analyze the use of random search techniques [32], [33], [34], [35], [36].

In this work, we consider nine publicly available benchmarks: three of iris printed spoofing attacks (Biosec [37], Warsaw [38], and MobBIOfake [39]), two of face (Replay-Attack [40] and 3DMAD [41]) and four of fingerprint spoofing attacks used in the latest, 2013, Fingerprint Liveness Detection Competition (LivDet'13) [11] (Biometrika, CrossMatch, Italdat, and Swipe). For all cases, our unified framework presents promising results across different biometric modalities.

It is worth mentioning that, recently, Galbally *et al.* [42] was one of the first authors to propose a unified countermeasure

method to detect spoofing attacks in face, iris, and fingerprint biometric systems. Their solution is based on image quality assessment. According to the authors, a spoofing attack can be detected by using 25 general image quality features extracted from one image. The experimental results reported attest the effectiveness of the method and its high competitiveness compared to other approaches. We see this work as the most related to ours, therefore, it is also worth mentioning a few key differences between these solutions. First and foremost, our method does not rely on image quality features, rather it automatically learns representational and discriminative features directly from the data using a deep learning framework. Second, our solution has been evaluated in more recent and updated databases which makes the comparison not straightforward. However, regardless of the differences, we believe that unified solutions for spoofing detection should be the path taken for future researchers in the field as they allow more generalizable models easing the integration of multi-biometrics solutions with multi-antispoofing solutions.

We organized the remainder of this work into five sections. Section II presents related work to the three biometric modalities of our interest (faces, fingerprints, and irises) while Section III presents the different datasets we consider for validation. Section IV introduces our methodology for spoofing attack detection under different modalities based on the optimization architectures of stacked layered CNNs. Section VI presents experimental results and comparisons with state-of-the-art methods. Finally, Section VII concludes the paper and shed light on some possible future research branches.

II. RELATED WORK

In this section, we review important works related to the spoofing biometric modalities addressed herein: iris, face and fingerprint.

A. Iris Spoofing

The feasibility of some attacks on iris recognition systems has been firstly reported, to the best of our knowledge, by Daugman [43, Section 8 – Countermeasures against Subterfuge]². That work proposed the use of Fast Fourier Transform to verify the high frequency spectral magnitude in the frequency domain. From the analysis of the iris patterns, it is possible to distinguish a printed iris image from a real one due to the characteristics of the periodic dot printing.

Several works dealing with different issues on iris liveness detection are available in the literature, ranging from active solutions that rely on special acquisition hardware [45], [46], [47] to software-based solutions such as the ones relying on texture analysis of the effects of an attacker using color contact lenses with someone else's pattern printed onto them [48]. The software-based solutions have also explored the effects of cosmetic contact lenses [49], [50], [9], [10]; pupil constriction [51]; and multi biometrics of electroencephalogram (EEG) and iris together [52], among others.

²It also appears in a lecture of Daugman at IBC 2004 [44].

Galbally et al. [53] investigated 22 image quality measures including focus, motion, occlusion, contrast, and pupil dilation. The best features are selected through sequential floating feature selection (SFFS) [54] to feed a quadratic discriminant classifier. The validation considered the BioSec [55], [37] database with a reported average error of 0.0%.

Also in the realm of image-based similarity, Sequeira et al. [56] used 14 features, SFFS [53] and three classification techniques. The validation introduced the MobBIOfake dataset comprising 800 iris images from the MobBIO multimodal database [39] and its correspondent fake high-quality printed copies captured with a handheld device. The reported misclassification rate was 12.50%. The authors examined the BioSec [55], [37] (0.37% misclassification rate) and Clarkson [14] (5.69%) datasets.

Sequeira et al. [57] extended upon previous works exploring quality measures. They first used a feature selection step on the features of the studied methods to obtain the “best features” and then used well-known classifiers for the decision-making. In addition, they applied iris segmentation [58] to obtaining the iris contour and adapted the feature extraction processes to the resulting non-circular iris regions. The validation considered five datasets (BioSec [55], [37], MobBIOfake [39], Warsaw [38], Clarkson [14] and NotreDame [59] – the latter two with contact lenses as fake images).

In a recent iris liveness competition, MobLive³ [8], an accuracy of 99.75% was achieved for the MobBIOfake dataset by the Indian Institute of Technology Indore team. Their approach analyzes three texture descriptors: Local Phase Quantization (LPQ) [60], Binary Gabor Pattern [61], and Local Binary Pattern (LBP) [62]. The solution combines the different evidence through fusion processes and performs the decision-making through SVMs with linear kernels.

Analyzing printing regularities left in printed irises, Czajka [38] explored some peaks in the frequency spectrum were associated to spoofing attacks. For localizing the peaks, the author sets up two disjoint frequency windows located under the iris. The window is used to observe the artifacts inserted during printing processing and the second window serves as a reference to the observed disturbances in an amplitude spectrum. Finally, a liveness score is calculated based on information from these two windows. The validation considered introduced the Warsaw dataset, which contains 729 fake images and 1,274 images of real eyes. In this dataset, it is claimed that the methodology can be set up to obtain no false alarms (0% of false rejection rate (FRR)) and 5% of false acceptance rate (FAR). In [14], The First Intl. Iris Liveness Competition in 2013, the Warsaw database was also evaluated, however, the best reported result achieved 11.95% of FRR and 5.25% of FAR by the University of Porto team.

Although not directly related to the datasets in our work, it is worthwhile to describe a recent work of Sun et al. [63], which proposed a general framework for iris image classification based on a Hierarchical Visual Codebook (HVC). The HVC encodes the texture primitives of iris images and is based on two existing bag-of-words models. The validation showed that

the proposed method achieved state-of-the-art performance for iris liveness detection, race classification and coarse-to-fine iris identification. Moreover, the authors also developed an iris image dataset with four types of fake iris patterns (iris texture printed on paper, plastic eyeballs, contact lens and synthetic fake iris images) called CASIA-Iris-Fake. The authors claimed that it is the first dataset comprising a large variety of fake iris patterns allowing an advance on the development of unified countermeasures against spoofing attacks.

B. Face Spoofing

Spoofing attack is easily performed against face biometrics systems due to low cost to produce a fake sample. As a matter of fact, there are excellent quality printers and digital cameras at a low price nowadays. In addition, the ease in obtaining facial information of a person through social networks and personal pages contributes for low-cost high-profit attacks.

We can categorize the face anti-spoofing methods into four groups [64]: user behavior modeling, methods relying on extra devices, methods relying on user cooperation and, finally, data-driven characterization methods. In this section, we review data-driven characterization methods proposed in literature, given such methods are preferable in practice because they do not require extra devices and neither do they need human involvement.

Määttä et al. [65] introduced an anti-spoofing method based on LBP operator able to capture printing artifacts and micro-texture patterns that are added in the fake biometric samples during acquisition. Schwartz et al. [64] proposed a method that extracts information of different properties of the images such as color, texture and shape of the face region and used them with Partial Least Square (PLS) classifier for deciding whether a biometric sample is fake or not. Results of these two techniques were reported in the Competition on Counter Measures to 2D Facial Spoofing Attacks [12], with a Half Total Error Rate (HTER) of 0.00% and 0.63%, respectively, upon the Print Attack database [66].

Pinto et al. [2] proposed visual rhythm analysis to capture temporal information on face spoofing attacks. During a video-based spoofing attack, a noise signature is added to the biometric samples during the recapture of the attack videos and can be used successfully to detect such attacks.

Lee et al. [67] explored frequency entropy of the images during attacks. Firstly, the face region is isolated and normalized using z -score. Thereafter, independent component analysis (ICA) is used to eliminate cross-channel noise caused by interference from the environment. Finally, the authors use the power spectrum and analyze the entropy of the RGB channels individually to further decide upon the attack based on an empirical threshold.

Mask-based face spoofing attacks have also been considered in the literature. Erdogmus et al. [68] explored a small database with six types of attacks using facial information of four subjects and proposed two algorithms based on Gabor wavelet: local Gabor binary pattern histogram sequences [69] and Gabor graphs [70] with a Gabor-phase based similarity measure [71]. Erdogmus & Marcel [41] introduced the 3D Mask

³MobLive 2014, Intl. Joint Conference on Biometrics (IJCB).

Attack database (3DMAD), a public available 3D spoofing database, recorded with Microsoft Kinect sensor. They also investigate the use of the LBP-based method and reported an HTER of 0.95% and 1.27% using the color and depth images, respectively.

Kose et al. [72] demonstrated that a face verification system is vulnerable to mask-based attacks and, in another work, Kose et al. [73] evaluated the anti-spoofing method proposed by Määttä et al. [65] (originally proposed to detect photo-based spoofing attacks). Inspired by the work of Tan et al. [74], Kose et al. [75] evaluated a solution based on reflectance to detect attacks performed with 3D masks. The authors reported an Area Under the Curve (AUC) of 97.0% and a classification accuracy of 94.47% using the non-public available MORPHO database [73].

Finally, Pereira et al. [76] proposed a score-level fusion strategy in order to detect various types of attacks. The authors trained classifiers using different databases and used the Q statistic to evaluate the dependency between classifiers. The combination of classifiers that are statistically independent leads to better results. In a follow-up work, Pereira et al. [77] proposed an anti-spoofing solution based on the dynamic texture, a spatio-temporal version of the original LBP. Results showed that LBP-based dynamic texture description has a higher effectiveness than the original LBP.

C. Fingerprint Spoofing

There are several approaches for fingerprint spoofing detection. We can categorize them into two groups: hardware-based and software-based solutions [11]. Methods following the first approach use information provided from additional sensors to gather artifacts that reveal a spoofing attack that are outside of the fingerprint image. Software-based techniques rely only on the information acquired by the standard acquisition sensor of the authentication system.

Galbally et al. [78] proposed a set of features for fingerprint liveness detection based on quality measures. The authors explored quality-based features such as ridge strength or directionality, ridge continuity, ridge clarity, and integrity of the ridge-valley structure. Such features are combined and a feature selection algorithm is used. The validation considered the three datasets used in LivDet 2009 – Fingerprint competition [7] – which were captured with different optical sensors: Biometrika, CrossMatch, and Identix. The authors reported an average error of 1.83%, 11.12%, and 6.73% using Biometrika, CrossMatch and Identix sets, respectively. Galbally et al. [79] also proposed to evaluate the previous method in the case in which the gummy fingers are generated with and without the cooperation of the user. The authors built a Biometrika.ATVS set using the Biometrika database from LivDet 2009 – Fingerprint competition, and obtained results showing that user cooperation may hinder spoofing attacks.

Ghiani et al. [80] explored LPQ [60], a method for representing all spectrum characteristics in a compact feature representation form for detecting liveness. The authors proposed a rotation-invariant version of LPQ, referenced as Rotation Invariant Local Phase Quantization (RILPQ). The

misclassification rate reported was 12.3% in the four databases used in the LivDet 2011 – Fingerprint competition [15]. A combination between proposed LPQ and LBP yielded even better results with a misclassification rate of 9.2% considering the LivDet 2011 – Fingerprint competition sets.

Gagnaniello et al. [81] explored the Weber Local Image Descriptor (WLD) for liveness detection, which appears to be very well suited to high-contrast patterns, such as the ridges and valleys of fingerprints images. In addition, WLD is robust to noise and illumination changes. The validation considered the LivDet 2009 and LivDet 2011 – Fingerprint competition datasets. The misclassification rates reported were 7.13% and 27.67%, respectively. When the proposed method is combined with RILPQ [82], the misclassification rates in both sets reduce to 3.13% and 12.65%, respectively.

Jia et al. [83] proposed a liveness detection scheme based on Multi-scale Block Local Ternary Patterns (MBLTP). Differently of the LBP, the Local Ternary Pattern operation is done on the average value of the block instead of the pixels, which makes it more robust to noise. Results obtained through LivDet 2011 – Fingerprint competition showed a misclassification rate lower than 10.0%.

Recently, Ghiani et al. [84] proposed a method for detecting fingerprint liveness based on Binarized Statistical Images Features (BSIF) method, originally proposed by Kannala et al. [85]. The BSIF was inspired in the LBP and LPQ methods, which describe each pixel neighborhood with a binary code obtained by first convolving the image with a set of linear filters and then binarizing the filter responses. In contrast to LBP and LPQ approaches, BSIF learns a filter set by using statistics of natural images [86]. The validation considered the datasets of the LivDet 2011 – Fingerprint competition yielding a misclassification rate of 7.22%.

Finally, recent results reported in the LivDet 2013 Fingerprint Liveness Detection Competition [84] show that fingerprint spoofing attack detection task is still an open problem. The competition attracted twelve academic and industrial institutions around the world. Even though good results have been achieved, they are still far from a perfect classification rate. The best classification results among four used datasets were achieved by one team of the University of Naples Federico II and another from the Dermalog Identification Systems. They reported an average accuracy of 86.63% and 84.63%, respectively.

III. BENCHMARKS

In this section, we describe the benchmarks/datasets we consider in this work. All used benchmarks are publicly available upon request and suitable for evaluating countermeasure methods to iris, face and fingerprint spoofing attacks. Table I shows the major features of each benchmark considered herein. In the following, we describe details of each dataset.

A. Live and Printed Spoofing Iris Benchmarks

1) *Biosec*: This dataset was created using iris images from 50 users of the BioSec [37]. In total, there are 16 images for each user (2 sessions \times 2 eyes \times 4 images), totalizing

TABLE I
MAIN FEATURES OF THE BENCHMARKS CONSIDERED HEREIN.

Modality	Benchmark/Dataset	Color	Dimension <i>cols × rows</i>	# Training			# Testing			# Development		
				Live	Fake	Total	Live	Fake	Total	Live	Fake	Total
Iris	Warsaw [38]	No	640 × 480	228	203	498	624	612	1236			
	Biosec [37]	Yes	640 × 480	200	200	400	600	600	1200			
	MobBIOfake [39]	Yes	250 × 200	400	400	800	400	400	800			
Face	Replay-Attack [12]	Yes	320 × 240	600	3000	3600	4000	800	4800	600	3000	3600
	3dMad [13]	Yes	640 × 480	350	350	700	250	250	500	250	250	500
Fingerprint	Biometrika [11]	No	315 × 372	1000	1000	2000	1000	1000	2000			
	CrossMatch [11]	No	800 × 750	1000	1000	2000	1000	1000	2000			
	Italdata [11]	No	640 × 480	1250	1000	2250	1250	1000	2250			
	Swipe [11]	No	208 × 1500	1221	979	2200	1153	1000	2153			

800 valid access images. To create the spoofing attacks, the original images from Biosec were preprocessed to improve the image quality and printed using an HP Deskjet 970cxi and an HP LaserJet 4200L printers. Finally, the iris images were recaptured with the same iris camera used to capture the original images.

2) *Warsaw*: This dataset contains 1274 iris images of 237 volunteers that represent valid accesses and 729 printout images that represent spoofing attacks, which were generated by using two printers: (1) a HP LaserJet 1320 used to produce 314 fake images with 600 dpi resolution, and (2) a Lexmark C534DN used to produce 415 fake images with 1200 dpi resolution. Both real and fake images were captured by an IrisGuard AD100 biometric device.

3) *MobBIOfake*: This dataset contains live iris images and spoof printed images captured with the same acquisition sensor, i.e., a handheld device (a cellphone). To generate fake images, the authors first performed a preprocessing in the original images to enhance the contrast. The preprocessed images were then printed with a professional printer on high quality photographic paper.

B. Video-based Face Attack Benchmarks

1) *Replay-Attack*: This dataset contains short video recordings of both valid accesses and attack videos of 50 different identities. To generate the valid access videos, each person was recorded in two sessions in a controlled and an adverse environment with a generic web cam. The attempted attacks were generated using three spoofing techniques: (1) *print attack*, which presents to the acquisition sensor hard copies of the high-resolution digital photographs printed using a Triumph-Adler DCC 2520 color laser printer; (2) *mobile attack*, which presents to the acquisition sensor photos and videos taken with an iPhone using the iPhone screen; and (3) *high-definition attack*, in which high resolution photos and videos taken with an iPad are presented to the acquisition sensor using the iPad screen.

2) *3DMAD*: This dataset comprises real access and mask attack videos of 17 different subjects recorded with a Microsoft Kinect sensor. The videos were collected in three sessions and, for each session and each person, five videos of 10 seconds were captured. The 3D masks for the attacks were produced by ThatsMyFace.com using one frontal and two profile images of each subject. To simulate spoofing attacks,

the authors were recorded wearing masks by same acquisition sensor used to capture the valid access videos.

C. Spoofing Fingerprint Benchmarks

1) *LivDet2013*: This dataset contains four sets of valid access and attempted spoofing performed in four acquisition sensors: Biometrika FX2000, Italdata ET10, Crossmatch L Scan Guardian, and Swipe. For a more realistic scenario, the fake samples in Biometrika and Italdata were generated without user cooperation, and the fake samples in Crossmatch and Swipe sets were generated with user cooperation. Several materials for creating the artificial fingerprints were used, including gelatin, silicone, latex, among others.

D. Remarks

The benchmarks described in this section aim at evaluating the proposed method considering a more realistic scenario, given that heterogeneity of the datasets is a challenge, mainly for algorithms based on machine learning, due to difficulty of finding a generalizable model. Even considering each modality alone, we have data from many different sensors, which complicates the problem of detecting an attempted attack, and different modes of spoofing attacks, using different types of equipment and procedures.

To have an idea of the difficulty of this problem, consider the images depicted in Fig. 2 (linked to Section VI). Observe the high variability even within the same modalities. Methods developed to work on some database using specific features might not perform well on other databases of the same problem. This hard scenario hints the use of the proposed framework which aims to learn deep representations from the data of each database such that promising effectiveness is expected to be achieved.

In the next section, we describe details of our framework for spoofing attack detection under different modalities. We shall return to the details in such figure when discussing the experimental results.

IV. FRAMEWORK FOR LEARNING DEEP REPRESENTATIONS

Our approach for learning deep representations builds on the work of Pinto et al. [32] and Bergstra et al. [36] in that fundamental, feedforward convolutional operations are stacked by means of hyperparameter optimization, leading to

effective yet simple convolutional neural networks (CNNs). In Section IV-A we present these operations and their hyperparameters. Sections IV-B and IV-C then describe how we stack these operations in layers and layers in CNNs. Finally, in Section IV-D we describe our procedure for combining CNN layers in order to extract good deep representations for the task at hand.

A. Fundamental Operations

Our networks use classic convolutional operations that can be viewed as linear and non-linear image processing operations. When stacked, these operations essentially extract higher level representations, named *multiband images*, whose pixel attributes are concatenated into high-dimensional feature vectors for later pattern recognition.⁴

Assuming $\hat{I} = (D_I, \vec{I})$ as a multiband image, where $D_I \subset Z^2$ is the image domain and $\vec{I}(p) = \{I_1(p), I_2(p), \dots, I_m(p)\}$ is the attribute vector of a m -band pixel $p = (x_p, y_p) \in D_I$, the aforementioned operations can be described as follows.

1) *Filter Bank Convolution*: Let $\mathcal{A}(p)$ be a squared region centered at p of size $L_A \times L_A$, such that $\mathcal{A} \subset D_I$ and $q \in \mathcal{A}(p)$ iff $\max(|x_q - x_p|, |y_q - y_p|) \leq (L_A - 1)/2$. Additionally, let $\Phi = (\mathcal{A}, W)$ be a filter with weights $W(q)$ associated with pixels $q \in \mathcal{A}(p)$. In the case of multiband filters, filter weights can be represented as vectors $\vec{W}_i(q) = \{w_{i,1}(q), w_{i,2}(q), \dots, w_{i,m}(q)\}$ for each filter i of the bank, and a multiband filter bank $\Phi = \{\Phi_1, \Phi_2, \dots, \Phi_n\}$ is a set of filters $\Phi_i = (\mathcal{A}, \vec{W}_i)$, $i = \{1, 2, \dots, n\}$.

The convolution between an input image \hat{I} and a filter Φ_i produces a band i of the filtered image $\vec{J} = (D_J, \vec{J})$, where $D_J \subset D_I$ and $\vec{J} = (J_1, J_2, \dots, J_n)$, such that for each $p \in D_J$,

$$J_i(p) = \sum_{\forall q \in \mathcal{A}(p)} \vec{I}(q) \cdot \vec{W}_i(q). \quad (1)$$

An important remark is that the weights of Φ_i are randomly generated from a uniform distribution, i.e., $U(0, 1)$, and are further normalized to zero mean and unit norm in order to ensure that they are spread over the unit sphere.

2) *Rectified Linear Activation*: The activation operation in our networks is performed by rectified linear units of the type present in many state-of-the-art CNN architectures [33], [21] and simply perform

$$J_i(p) = \max(J_i(p), 0). \quad (2)$$

Notwithstanding its simplicity, this activation function plays an important role in the network information flow, specially when coupled with random filters initialized as described above, in which case it enforces sparsity in the network by discarding 50% of the expected filter responses, thereby improving the overall robustness of the features being extracted.

3) *Spatial Pooling*: Spatial pooling is an operation of paramount importance in the CNN literature [25] that aims at bringing translational invariance to the features by aggregating activations from the same filter in a given region.

Let $\mathcal{B}(p)$ be a pooling region of size $L_B \times L_B$ centered at pixel p and $D_K = D_J/s$ be a regular subsampling of every s pixels $p \in D_J$. We call s the *stride* of the pooling operation. Given that $D_J \subset Z^2$, if $s = 2$, $|D_K| = |D_J|/4$, for example. The pooling operation resulting in the image $\hat{K} = (D_K, \vec{K})$ is defined as

$$K_i(p) = \sqrt[\alpha]{\sum_{\forall q \in \mathcal{B}(p)} J_i(q)^\alpha}, \quad (3)$$

where $p \in D_K$ are pixels in the new image, $i = \{1, 2, \dots, n\}$ are the image bands, and α is a hyperparameter that controls the sensitivity of the operation. In other words, our pooling operation is the L_α -norm of values in $\mathcal{B}(p)$. The stride s and the pooling neighborhood defined by L_B are other hyperparameters of this operation.

4) *Divisive Normalization*: The last operation that we consider in our CNNs is the divisive normalization, a mechanism widely used in top-performing CNNs [33], [21] that is based on gain control mechanisms found in cortical neurons [87].

This operation is also defined within a squared region $\mathcal{C}(p)$ of size $L_C \times L_C$ centered at pixel p such that

$$O_i(p) = \frac{K_i(p)}{\sqrt{\sum_{j=1}^n \sum_{\forall q \in \mathcal{C}(p)} K_j(q) \cdot K_j(q)}} \quad (4)$$

for each pixel $p \in D_O \subset D_K$ of the resulting image $\hat{O} = (D_O, \vec{O})$. Divisive normalization promotes competition among pooled filters bands such that high responses will prevail even more over low ones, further strengthening the robustness of the CNN output feature vector \vec{O} .

B. Stacking Operations in a Layer

As presented in Fig. 1(a), we denote by *one layer* the combination of the four previously presented operations in the order that they appear. Indeed, *divisive normalization* is optional and its use is governed by one out seven hyperparameters present in each layer and detailed as follows:

- L_A filter size;
- n number of filters;
- L_B pooling size;
- s pooling stride;
- α pooling sensitivity;
- ln_{choice} apply layer normalization (yes/no);
- L_C normalization size (as conditioned above).

C. Stacking Layers in a CNN

As already mentioned, a single layer in our network has seven hyperparameters. Here we are interesting in learning deep representations through the combination of several layers, which substantially increases the number hyperparameters.

⁴In this paper, CNNs are described from an image processing perspective, with terms like image *domain*, image *band*, etc., used throughout.

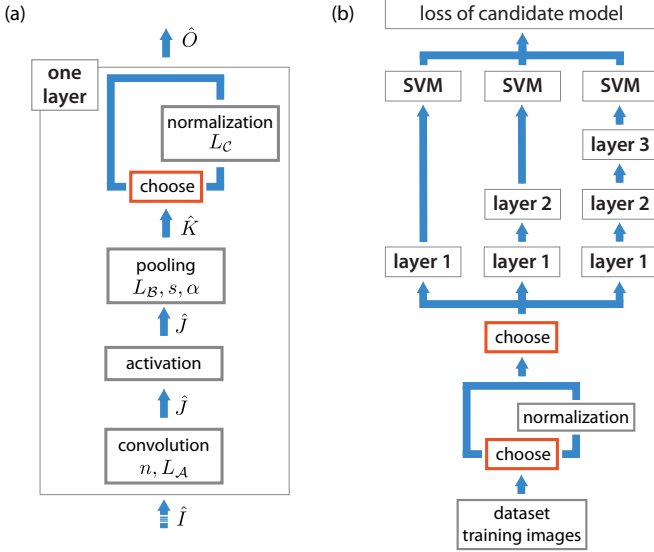


Fig. 1. A schematic representation of the proposed framework illustrating how the four fundamental operations are stacked in a layer (a) and how the network is governed and evaluated according to the hyperparameter values (b). Note that a three-layered CNN of this type has a total of 25 hyperparameters determining its architecture and behavior.

Indeed, aside from the hyperparameters of each layer, our networks additionally have the following *global* hyperparameters:

- \max_{axis} resize images so as the number of rows and columns are limited to this value while the aspect ratio is kept;
- in_{choice} apply input normalization (yes/no);
- L_C normalization size (as conditioned above);
- d_{choice} number of layers.

Fig. 1(b) illustrates these hyperparameters and how they influence the network depth and information flow. A three-layered CNN of this type, for example, has a total of 25 hyperparameters determining its architecture and behavior.

D. Representation Learning via Hyperparameter Optimization

The set of hyperparameters considered lie in a space which is difficult to search, comprising both discrete and continuous variables as well as conditioned variables that are only meaningful for some combinations of other variables.

In spite of the intrinsic difficulty, *random search* has played an important role in addressing problems of this type [32], [34]. Due to its effectiveness and simplicity, this is our strategy of choice for learning good deep representations here. Basically, we define a search space comprising possible, discrete values for all hyperparameters and search for the CNN producing the best representation according to a particular performance measure. The algorithm can be described as follows:

- 1) Randomly — and uniformly, in our case — sample values from the CNN hyperparameter *search space*;

- 2) Extract features from the dataset training images with this CNN;
- 3) Evaluate the CNN according to an *optimization objective*;
- 4) Repeat steps 1–3 until a *termination criterion* is met;
- 5) Return the best CNN.

The hyperparameter search space, optimization objective, and termination criterion used in this work are described in the next section.

V. EXPERIMENTAL SETUP

Besides presenting the experimental setup of the hyperparameter optimization, in this section, we describe elementary data preprocessing done on the image benchmarks used in the experiments and also the evaluation protocol used to report the final effectiveness of our proposed frame.

A. Hyperparameter Optimization

1) *Search Space*: We define a discrete hyperparameter search space based on previous work [33], [36] and experience. In accordance to the notation used in Section IV, values for each variable are sampled with equal probability according to the following options:

- *network-wise*
 - \max_{axis} {64, 128, 256, *original size*};
 - in_{choice} {yes, no};
 - L_C {3, 5, 7, 9};
 - d_{choice} {1, 2, 3};
- *layer-wise*
 - L_A {3, 5, 7, 9};
 - n {32, 64, 128, 256};
 - L_B {3, 5, 7, 9};
 - s {1, 2, 4, 8};
 - α {1, 2, 10};
 - ln_{choice} {yes, no};
 - L_C {3, 5, 7, 9};

Even though the hyperparameter search space may seem small, it is possible to observe from the values of d_{choice} that we consider networks of up to three layers. Therefore, a total of 25 hyperparameters — spanning a set of over 70 billion possible networks — are considered in the optimization. However, not all candidate networks are valid. For example, a large number of candidate architectures (i.e., points in the hyperparameter space) would produce representations with spatial resolution smaller than one pixel. Hence, they are naturally unfeasible. We additionally impose two restrictions to the set of valid CNNs in order to avoid very large representations. Specifically, we discard candidate CNNs whose intermediate layers produce representations of over 600K elements or whose output representation has over 30K elements.

2) *Optimization Objective*: We evaluate the performance of a candidate CNN by first extracting deep representations from the training samples of a given benchmark and later performing 10-run validation instead of the traditional 10-fold cross-validation (CV) on these features with hard-margin

TABLE II
INPUT IMAGE DIMENSIONALITY AFTER BASIC PREPROCESSING ON FACE
AND FINGERPRINT IMAGES (HIGHLIGHTED). SEE SECTION V-B FOR
DETAILS.

Modality	Benchmark	Dimensions <i>columns × rows</i>
Iris	Warsaw [38]	640 × 480
	Biosec [37]	640 × 480
	MobBIOfake [39]	250 × 200
Face	Replay-Attack [12]	200 × 200
	3DMAD [13]	200 × 200
Fingerprint	Biometrika [11]	218 × 260
	CrossMatch [11]	480 × 675
	Italdata [11]	384 × 432
	Swipe [11]	187 × 962

linear SVMs ($C=10^5$). We opted for different *training* and *validation* splits. Instead of training on nine folds and validating on one as the traditional CV protocol, we train on one fold and validate on nine. This strategy was adopted in order to improve the sensitivity of the performance measure which, in some benchmarks was saturating with traditional 10-fold CV. Precisely, the optimization objective is the mean detection accuracy obtained from cross-validation, which is maximized during the optimization.

For generating the 10 folds, it is important to observe that we took special care in putting all samples of an individual in the same fold to enforce robustness to cross-individual spoofing attacks in the CNNs. Moreover, in benchmarks where we have more than one attack type — Replay-Attack and LivDet2013 (see Section III) — we evenly distributed samples of each attack type across all folds in order to enforce that candidate CNNs are also robust to different types of attack.

3) *Termination Criterion*: The termination criterion is the last definition that remains to be given to complete the optimization procedure presented in Section IV-D. In this work, it simply consists of counting the number of valid candidate CNNs and stopping the optimization when this number reaches 2,000.

B. Elementary Data Preprocessing

Beyond converting all images to grayscale, a few basic preprocessing operations were executed on face and iris images in order to properly learn representations for these benchmarks. This preprocessing led to images with sizes as presented in Table II and are described in the next two sections.

1) *Face Images*: Given that the face datasets considered in this work are video-based, we first evenly subsample 10 frames from each input video. Then, we detect the face position using Viola & Jones [88] and crop a region of 200×200 pixels centered at the detected window.

2) *Fingerprint Images*: Given the diverse nature of images captured from different sensors, here the preprocessing is defined according to the sensor type.

- (a) *Biometrika*: we cropped the central region of size in columns and rows corresponding to 70% of the original image dimensions.
- (b) *Italdata* and *CrossMatch*: we cropped the central region of size in columns and rows respectively corresponding to 60% and 90% of the original image columns and rows.

- (c) *Swipe*: As the images acquired by this sensor contain a variable number of blank rows at the bottom, the average number of non-blank rows M was first calculated from the training images. Then, in order to obtain images of a common size with non-blank rows, we removed their blank rows at the bottom and rescaled them to M rows. Finally, we cropped the central region corresponding to 90% of original image columns and M rows.

The rationale for these operations is based on the observation that fingerprint images in LivDet2013 tend to have a large portion of background content and therefore we try to discard such information that could otherwise mislead the representation learning process. The percentage of cropped columns and rows differs among sensors because they capture images of different sizes with different amounts of background.

C. Evaluation Protocol

For each benchmark, we learn deep representations from their training images according to the procedure described in Section IV-D and the setup given in Section V-A. We follow the standard evaluation protocol of all datasets and evaluate the framework both in terms of detection accuracy (ACC) and half total error rate (HTER), as these are the metrics used to assess progress in the set of benchmarks here considered. More precisely, the results are obtained by:

- 1) Extracting deep representations from all images in the benchmark with the best CNN found in the hyperparameter optimization;
- 2) Training a hard-margin ($C=10^5$) linear SVM on these representations;
- 3) Calculating a threshold τ above which samples are predicted as attacks;
- 4) Computing ACC and HTER from the benchmark testing set using the SVM predictions and τ .

The way that τ is calculated differs depending on whether the benchmark has a development set or not (Table I). The face benchmarks have such a set, and in this case we simply obtain τ from the predictions of the samples in this set. The iris and fingerprint benchmarks have no such a set. In this case, we calculate τ by joining the predictions obtained from 10-run cross-validation, instead of a traditional 10-fold cross-validation — performed the same way as described in Section V-A2 — in a single set of positive and negative scores. In all cases, τ is computed as the point that lead to an equal error rate (EER) on the score distribution under consideration. ACC and HTER are then trivially computed with τ on the testing set.

It is worth noting that the Warsaw iris benchmark provides a supplementary testing set that here we merge with the original testing set in order to replicate the protocol of [14]. Moreover, given that the face benchmarks are video-based and in our framework we treat them as images (Section V-B), we perform a score-level fusion of the samples from the same video according to the max rule [89]. This fusion is done before calculating τ . Finally, note that the classification engine here used is the same as the one used in the representation learning process, which enables a direct assessment on how

TABLE III

OVERALL RESULTS CONSIDERING KEY INFORMATION FROM THE BEST CNN FOUND, DETECTION ACCURACY (ACC) AND HTER OBTAINED ACCORDING TO THE EVALUATION PROTOCOL, AND THE STATE-OF-THE-ART (SOTA) IN THESE BENCHMARKS AVAILABLE IN THE LITERATURE.

Modality	Database	Optimization Step					Our Results		SOTA Results		
		time (secs.)	\max_{axis} (pixels)	layers (#)	features (#)	objective (%)	ACC (%)	HTER (%)	ACC (%)	HTER (%)	Ref.
Iris	Warsaw	52+35	640	2	$10 \times 15 \times 64$ (9600)	98.21	99.84	0.16	97.50	—	[38]
	Biosec	80+34	640	3	$2 \times 5 \times 256$ (2560)	97.56	98.83	1.17	100.00	—	[53]
	MobBIOfake	18+37	250	2	$5 \times 7 \times 256$ (8960)	98.94	98.63	1.38	99.75	—	[8]
Face	Replay-Attack	33+13	256	2	$4 \times 4 \times 128$ (2048)	89.64	88.71	9.38	—	5.11	[13]
	3DMAD	55+15	128	2	$5 \times 5 \times 64$ (1600)	98.68	100.00	0.00	—	0.95	[68]
Fingerprint	Biometrika	66+25	256	2	$2 \times 2 \times 256$ (1024)	90.11	96.50	3.50	98.30	—	[11]
	Crossmatch	112+12	675	3	$2 \times 3 \times 256$ (1536)	91.70	92.09	8.44	68.80	—	[11]
	Italdata	46+27	432	3	$16 \times 13 \times 128$ (26624)	86.89	97.45	2.55	99.40	—	[11]
	Swipe	97+51	962	2	$53 \times 3 \times 32$ (5088)	90.32	88.94	11.47	96.47	—	[11]

generalizable the representations learned with the framework are.

D. Implementation and Hardware Details

Our implementation is based on HyperOpt-Convnet [90] which in turn is based on Theano [91]. LibSVM [31] is used for learning the linear classifiers via Scikit-learn.⁵ The code for feature extraction runs on GPUs due to Theano — which is fundamental in becoming CNN hyperparameter optimization practical — and the remaining part of the framework is multi-threaded and runs on CPUs. We extended HyperOpt-Convnet in order to consider the operations and hyperparameters as described in Section IV and we will make the source code to reproduce this work freely available in [92] upon acceptance of the paper.

Running times are reported following this combination. Specifically, they are all computed in an Intel i7 @3.5GHz with a Tesla K40 that, on average, takes less than one day to learn a representation — i.e., to probe 2,000 CNNs — for a given benchmark. In a similar CPU setup, we also run experiments with other GPUs, such as GeForce Titan Black and GeForce GTX 680 and though they were slower than Tesla K40, the runtime is not fifty percent and twice times bigger, respectively, than the one took by the CPU using the Tesla K40 GPU.

VI. RESULTS AND DISCUSSION

In this section, we evaluate and discuss the effectiveness of the proposed framework for detecting iris, face, and fingerprint spoofing attack attempts on the nine benchmarks of Section III. Results are reported as described in Section V-C along with information regarding the representation learning process.

Table III shows the overall results and is divided in three parts. In the first part, we present key aspects of the best CNNs found in the hyperparameter optimization step, reporting the time (in seconds) demanded to evaluate it (feature extraction + 10-run validation), the input size that the CNN assumes (\max_{axis}), its depth (d_{choice}), and the dimensionality of its output representations in terms of $columns \times rows \times bands$.

The results obtained according to the evaluation protocol are shown in the second part of Table III and a direct comparison

of these numbers with the state-of-the-art (SOTA) can be made considering its third part.

The first thing to notice in Table III is the time required to evaluate the best CNNs on the respective benchmark training sets. We can see, for example, that the most computationally intensive representation is the one found for the Swipe benchmark, and demanded 148 seconds to process 2,200 images. Such a running time was only possible due to the GPU+CPU implementation used (Section V-D), which is critical for this type of learning task. In a hypothetical operational scenario, we could ignore the time required to train the linear classifiers. Indeed, once a system is trained, prediction requires a single dot product, and the time demanded for this operation is negligible. Therefore, we can estimate that, on average, a single image captured by a Swipe sensor would require approximately 45 milliseconds — plus a little overhead — to be fully processed in this hypothetical system.

Regarding the number of layers required by the CNNs producing the best representations, we can observe that six out of nine CNNs use two layers, and three CNNs use three layers. We speculate that the number of layers obtained is a function of the problem complexity. Even though there are many other hyperparameters involved, the number of layers play an important role in this issue, since it directly influences the level of non-linearity and abstraction of the output with respect to the input.

With respect to the input image size (\max_{axis}), we can see in comparison with Table II that the best performing CNNs often use the original image size. This was the case for all iris benchmarks and for three (out of four) fingerprint benchmarks. For the face benchmarks, a larger input was preferred for Replay-Attack, while a smaller input was preferred for 3DMAD. We hypothesize that this is also related to the problem difficulty, given that Replay-Attack seems to be more difficult, and that larger inputs tend to lead to larger networks.

Still with respect to the outcomes of the optimization, we notice that the dimensionality of the obtained representations are, in general, smaller than 10K features, except for Italdata. Moreover, for the face and iris benchmarks, it is possible to roughly observe a relationship between the optimization objective calculated in the training set (Section V-A2) and the detection accuracy measure on the testing set (Section V-C), which indicates the appropriateness of the objective for these tasks. However, for the fingerprint benchmarks, this relation-

⁵<http://scikit-learn.org>

TABLE IV

COMPARISON OF OUR FRAMEWORK RESULTS WITH THE ONES OF THE LIVDET'2013 - FINGERPRINT LIVENESS DETECTION COMPETITION

Databases	Accuracy in %				
	Ours	Dermalog	Anonym1	UniNap1	Overall Best
Biometrika	96.50	98.30	98.20	95.30	98.30
CrossMatch	92.09	44.53	45.29	68.80	68.80
Italdat	97.45	99.20	99.40	96.50	99.40
Swipe	88.94	96.47	94.19	85.93	96.47
Average	93.75	84.63	84.25	86.63	90.74

ship does not exist, and we attribute this to either a deficiency of the optimization objective in modeling these problems or the existence of artifacts in the training set misleading the optimization.

From the second and third parts of Table III, we can see that the performance of our systems are very competitive. In fact, by training simple linear classifiers on the deep representations found with our framework, our systems were able to outperform three SOTA methods and performed close to other four methods. In particular, we obtained state-of-the-art performance on the Warsaw, 3DMAD, and CrossMatch benchmarks, each one of a different biometric trait: iris, face, and fingerprint, respectively. The two benchmarks where our approach was less successful are Replay-Attack and Swipe, but even in these cases the performance of our systems was acceptable.

Putting our fingerprint results in another perspective, in Table IV we repeat them and include results obtained from three teams that participated in the Fingerprint Liveness Detection Competition [11] — or LivDet2013 — whose methods are the current state-of-the-art on at least one of the benchmarks. These teams are Dermalog, Anonym1, and UniNap1. As we can see, Dermalog and Anonym1 achieve very good results on three benchmarks, but perform poorly on Crossmatch, even worse than random guess. The UniNap1 method is the SOTA on Crossmatch, but its performance is still poor. In contrast, our framework yields consistent detection accuracies on the four benchmarks, obtaining an average accuracy of 93.75%, which is better than the average performance of any other team, and better even if we consider the combination of all SOTA methods.

In Fig. 2, we show examples of hit and missed testing samples lying closest to the real-fake decision boundary of each benchmark. A magnified visual inspection on these images may give us some hint about properties of the problem to which the learned representations are sensitive.

While it is difficult to infer anything concrete, it is interesting to see that the real missed sample in Biosec is quite bright, and that skin texture is almost absent in this case. Still, we may argue that a possible reason for the fake miss in MobBIOfake is the use of glasses, and that a noticeable difference exists in Warsaw between the resolution used to print the images that led to the fake hit and the fake miss. Regarding the face benchmarks, the only noticeable observation from Replay-Attack is that the same person is missed both when providing to the system a real and a fake biometric reading. This may indicate that some individuals are

more likely to successfully attack a face recognition systems than others. In 3DMAD, it is easy to see the difference between the real and fake hits. Notice that there was no misses in this benchmark.

A similar visual inspection is much harder in the fingerprint benchmarks, even though the learned deep representations could effectively characterize these problems. The only observation possible to be made here is related to the fake hit on CrossMatch, which is clearly abnormal. The images captured with the Swipe sensor are naturally narrow and distorted due to the process of acquisition, and this distortion prevents any such observations.

VII. CONCLUSIONS AND FUTURE WORK

In this work, we proposed a unified framework for the detection of iris, face, and fingerprint spoofing attacks by learning representations directly from the data with a final linear SVM classifier atop the representations. Experiments showed that our framework achieved not only promising but very competitive classification results for all problems and modalities and, in some cases, state-of-the-art results.

We emphasize the robustness and simplicity of the framework. Although it is more computationally expensive than some existing custom-tailored solutions, our approach is robust to learn representations directly from the data and this is a powerful way of dealing with big data. The more data we can collect over time across different modalities, the better and more discriminative will be the representation learning and, consequently, the decision-making process. Moreover, the very fact that the representations are learned directly from the data implies that there is no need for a specialist in each modality or databases for achieving promising results or even outperforming the state-of-the-art methods. If specialist knowledge is available, it can be combined with the proposed solution to provide better-quality training samples and push the solution even further.

The unified framework can also be adapted for other object verification and/or identification applications and can consider other biometric modalities not directly dealt with herein. The framework described here for CNNs optimization aiming at biometric spoofing detection involves the use of labeled databases and their evaluation protocol. Moreover we focused on devising and developing a simple framework. We could have used even more advanced pattern recognition/machine learning techniques such as data augmentation [21], space feature reduction/selection [18] and more elaborated classifiers, for increasing the effectiveness of the obtained methods.

Finally, for the case of iris spoofing detection, here we dealt only with iris spoofing printed attacks and some experimental datasets using cosmetic contact lenses have recently become available allowing researchers to study this specific type of spoofing [9], [10]. For future work, we intend to incorporate such datasets in our framework and also consider other biometric modalities such as palm, vein, and gait.

ACKNOWLEDGMENT

We thank UFOP, Brazilian National Research Council — CNPq (Grants #303673/2010-9, #304352/2012-8,

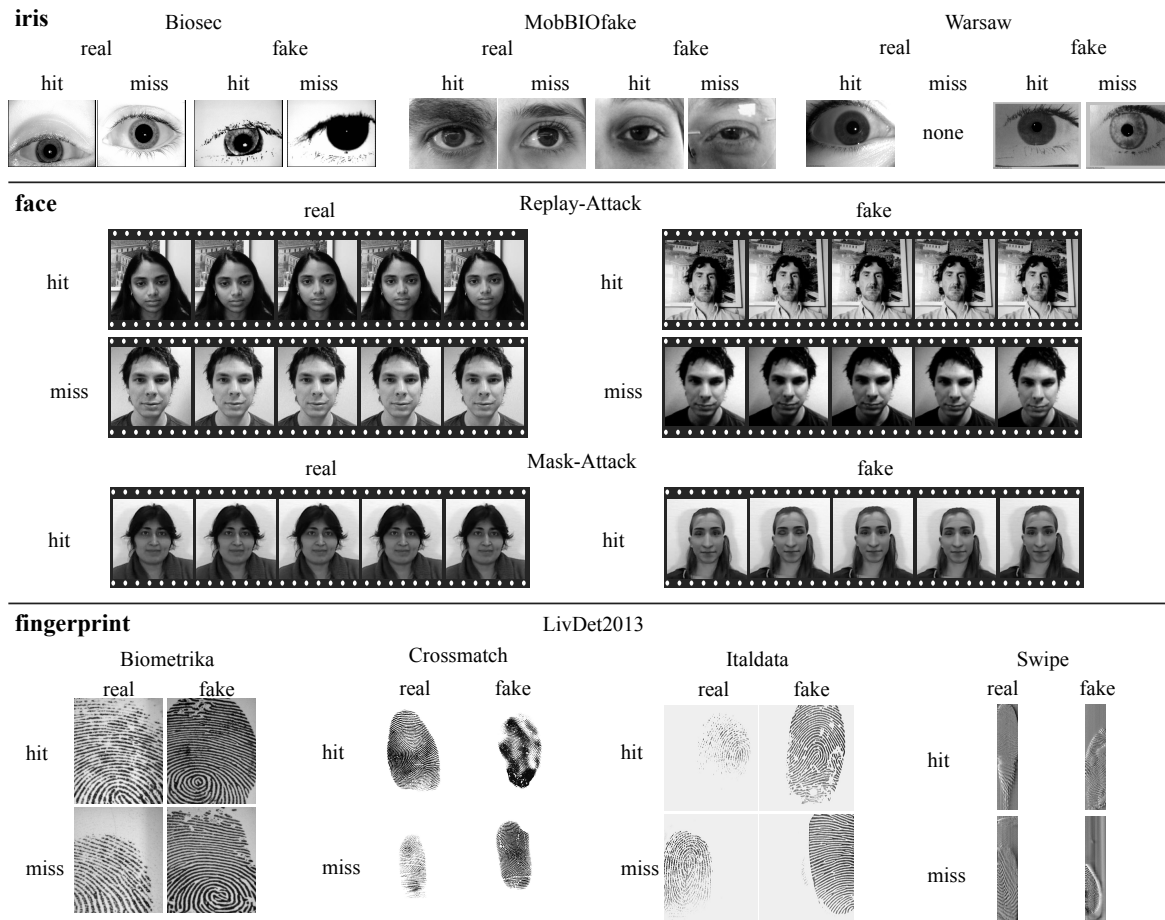


Fig. 2. Examples of hit and missed testing samples lying closest to the real-fake decision boundary of each benchmark. A magnified visual inspection on these images may suggest some properties of the problem to which the learned representations are sensitive.

#307113/2012-4, #477662/2013-7, #487529/2013-8, and #479070/2013-0), São Paulo Research Foundation – FAPESP, (Grants #2010/05647-4, #2011/22749-8, #2013/04172-0, and #2013/11359-0), and Minas Gerais Research Foundation - FAPEMIG (Grant APQ-#01806-13). D. Menotti thanks FAPESP for a grant for acquiring two NVIDIA GeForce Titan Blacks with 6 Gb each. We also thank NVIDIA corporation for donating three GPUS, a Tesla K40 with 12 Gb to A. X. Falcão, and two GeForce GTX 680 with 2Gb each to G. Chiachia with which we conducted the experiments herein.

REFERENCES

- [1] A. K. Jain and A. Ross, *Handbook of Biometrics*. Springer, 2008, ch. Introduction to biometrics, pp. 1–22.
- [2] A. Pinto, H. Pedrini, W. R. Schwartz, and A. Rocha, “Video-based face spoofing detection through visual rhythm analysis,” in *Conference on Graphics, Patterns and Images (SIBGRAPI)*, 2012, pp. 221–228.
- [3] C. Rathgeb and A. Uhl, “Attacking iris recognition: An efficient hill-climbing technique,” in *IEEE/IAPR International Conference on Pattern Recognition (ICPR)*, 2010, pp. 1217–1220.
- [4] —, “Statistical attack against iris-biometric fuzzy commitment schemes,” in *IEEE Computer Society Conference on Computer Vision and Pattern Recognition Workshops (CVPRW)*, 2011, pp. 23–30.
- [5] J. Galbally, J. Fierrez, and J. Ortega-garcia, “Vulnerabilities in biometric systems: Attacks and recent advances in liveness detection,” *Database*, vol. 1, no. 3, pp. 1–8, 2007, available at http://atvs.ii.uam.es/files/2007_SWB_VulnerabilitiesRecentAdvances_Galbally.pdf.
- [6] N. K. Ratha, J. H. Connell, and R. M. Bolle, “An analysis of minutiae matching strength,” in *International Conference on Audio-and Video-Based Biometric Person Authentication*, 2001, pp. 223–228.
- [7] G. L. Marcialis, A. Lewicke, B. Tan, P. Coli, D. Grimbey, A. Congiu, A. Tidu, F. Roli, and S. A. C. Schuckers, “Livdet 2009 – first international fingerprint liveness detection competition,” in *Int. Conference on Image Analysis and Processing (ICIAP)*, ser. Lecture Notes in Computer Science, P. Foggia, C. Sansone, and M. Vento, Eds., vol. 5716. Springer, 2009, pp. 12–23. [Online]. Available: <http://prag.diee.unica.it/LivDet09>
- [8] A. F. Sequeira, J. C. Monteiro, H. P. Oliveira, and J. S. Cardoso, “Mobilive 2014 - Mobile Iris Liveness Detection Competition,” in *IEEE Int. Joint Conference on Biometrics (IJCB)*, 2014, accepted for publication. [Online]. Available: <http://mobilive2014.inescporto.pt/>
- [9] K. W. Bowyer and J. S. Doyle, “Cosmetic contact lenses and iris recognition spoofing,” *Computer*, vol. 47, no. 5, pp. 96–98, 2014.
- [10] D. Yadav, N. Kohli, J. Doyle, R. Singh, M. Vatsa, and K. Bowyer, “Unraveling the effect of textured contact lenses on iris recognition,” *IEEE Trans. Inf. Forens. Security*, vol. 9, no. 5, pp. 851–862, 2014.
- [11] L. Ghiani, D. Yambay, V. Mura, S. Tocco, G. Marcialis, F. Roli, and S. Schuckers, “Livdet 2013 – fingerprint liveness detection competition,” in *International Conference on Biometrics (ICB)*, 2013, pp. 1–6. [Online]. Available: <http://prag.diee.unica.it/fldc/>
- [12] M. Chakka, A. Anjos, S. Marcel, R. Tronci, D. Muntoni, G. Fadda, M. Pili, N. Sirena, G. Murgia, M. Ristori, F. Roli, J. Yan, D. Yi, Z. Lei, Z. Zhang, S. Li, W. Schwartz, A. Rocha, H. Pedrini, J. Lorenzo-Navarro, M. Castrillon-Santana, J. Maatta, A. Hadid, and M. Pietikainen, “Competition on counter measures to 2-d facial spoofing attacks,” in *IEEE Int. Joint Conference on Biometrics (IJCB)*, 2011, pp. 1–6.
- [13] I. Chingovska, J. Yang, Z. Lei, D. Yi, S. Li, O. Kahm, C. Glaser, N. Damer, A. Kuijper, A. Nouak, J. Komulainen, T. Pereira, S. Gupta, S. Khandelwal, S. Bansal, A. Rai, T. Krishna, D. Goyal, M.-A. Waris,

- H. Zhang, I. Ahmad, S. Kiranyaz, M. Gabbouj, R. Tronci, M. Pili, N. Sirena, F. Roli, J. Galbally, J. Fierrez, A. Pinto, H. Pedrini, W. Schwartz, A. Rocha, A. Anjos, and S. Marcel, "The 2nd competition on counter measures to 2d face spoofing attacks," in *IAPR Int. Conference on Biometrics (ICB)*, 2013, pp. 1–6.
- [14] S. Schuckers, K. Bowyer, A. C., and D. Yambay, "Livdet 2013 - liveness detection iris competition," 2013. [Online]. Available: <http://people.clarkson.edu/projects/biosal/iris/>
- [15] D. Yambay, L. Ghiani, P. Denti, G. Marcialis, F. Roli, and S. Schuckers, "Livdet 2011 - fingerprint liveness detection competition," in *IAPR Int. Conference on Biometrics (ICB)*, 2012, pp. 208–215. [Online]. Available: <http://people.clarkson.edu/projects/biosal/fingerprint/index.php>
- [16] Y. Bengio, A. Courville, and P. Vincent, "Representation learning: A review and new perspectives," *Pattern Analysis and Machine Intelligence, IEEE Transactions on*, vol. 35, no. 8, pp. 1798–1828, 2013.
- [17] N. Pinto, Z. Stone, T. Zickler, and D. D. Cox, "Scaling up biologically-inspired computer vision: a case study in unconstrained face recognition on facebook," in *IEEE Computer Society Conference on Computer Vision and Pattern Recognition Workshops (CVPRW)*, 2011, pp. 35–42.
- [18] G. Chiachia, N. Pinto, W. Schwartz, A. Rocha, A. X. Falcão, and D. Cox, "Person-specific subspace analysis for unconstrained familiar face identification," in *British Machine Vision Conference (BMVC)*, 2012, pp. 1–12.
- [19] G. Chiachia, A. X. Falcão, N. Pinto, A. Rocha, and D. Cox, "Learning person-specific face representation," *IEEE Trans. Inf. Forens. Security*, 2014, accepted for publication.
- [20] D. C. Ciresan, U. Meier, L. M. Gambardella, and J. Schmidhuber, "Deep big simple neural nets for handwritten digit recognition," *Neural Computation*, vol. 22, no. 12, pp. 3207–3220, 2010.
- [21] A. Krizhevsky, I. Sutskever, and G. E. Hinton, "ImageNet Classification with Deep Convolutional Neural Networks," in *Advances in Neural Information Processing Systems (NIPS)*, 2012.
- [22] D. Ciresan, U. Meier, J. Masci, and J. Schmidhuber, "Multi-column deep neural network for traffic sign classification," *Neural Networks*, vol. 20, no. 1, 2012.
- [23] J. Ouyang and X. Wang, "Joint deep learning for pedestrian detection," in *International Conference on Computer Vision (ICCV)*, 2014.
- [24] Y. Taigman, M. Yang, M. Ranzato, and L. Wolf, "Deepface: Closing the gap to human-level performance in face verification," in *IEEE International Conference on Computer Vision and Pattern Recognition*, 2014.
- [25] Y. LeCun, L. Bottou, Y. Bengio, and P. Haffner, "Gradient-based learning applied to document recognition," *Proceedings of the IEEE*, vol. 86, no. 11, pp. 2278–2324, 1998.
- [26] K. Jarrett, K. Kavukcuoglu, M. Ranzato, and Y. LeCun, "What is the Best Multi-Stage Architecture for Object Recognition?" in *IEEE International Conference on Computer Vision*, 2009, pp. 2146–2153.
- [27] A. Coates and A. Ng, "The Importance of Encoding Versus Training with Sparse Coding and Vector Quantization," in *International Conference on Machine Learning (ICML)*, 2011, pp. 921–928.
- [28] Q. Le, M. Ranzato, R. Monga, M. Devin, K. Chen, G. Corrado, J. Dean, and A. Y. Ng, "Building high-level features using large scale unsupervised learning," in *International Conference in Machine Learning*, 2012, pp. 1–11.
- [29] A. Coates, B. Huval, T. Wang, D. J. Wu, A. Y. Ng, and B. Catanzaro, "Deep Learning with COTS HPC," in *International Conference on Machine Learning (ICML)*, 2013, pp. 1337–1345.
- [30] C. Cortes and V. N. Vapnik, "Support-vector networks," *Machine Learning*, vol. 20, no. 3, pp. 273–297, 1995.
- [31] C.-C. Chang and C.-J. Lin., "LIBSVM: a library for support vector machines," *ACM Transactions on Intelligent Systems and Technology*, vol. 2, no. 3, pp. 1–27, 2011.
- [32] N. Pinto, D. Doukhan, J. J. DiCarlo, and D. D. Cox, "A high-throughput screening approach to discovering good forms of biologically-inspired visual representation," *PLoS Computational Biology*, vol. 5, no. 11, p. e1000579, 2009.
- [33] N. Pinto and D. D. Cox, "Beyond simple features: A large-scale feature search approach to unconstrained face recognition," in *IEEE Int. Conference and Workshops on Automatic Face and Gesture Recognition (FG)*, 2011, pp. 8–15.
- [34] J. Bergstra and Y. Bengio, "Random search for hyper-parameter optimization," vol. 13, pp. 281–305, 2012.
- [35] J. Bergstra, R. Bardenet, Y. Bengio, and B. Kégl, "Algorithms for hyper-parameter optimization," in *Advances in Neural Information Processing Systems (NIPS)*, 2011, pp. 2546–2554.
- [36] J. Bergstra, D. Yamins, and D. D. Cox, "Making a Science of Model Search: Hyperparameter Optimization in Hundreds of Dimensions for Vision Architectures," in *International Conference on Machine Learning*, 2013.
- [37] V. Ruiz-Albacete, P. Tome-Gonzalez, F. Alonso-Fernandez, J. Galbally, J. Fierrez, and J. Ortega-Garcia, "Direct attacks using fake images in iris verification," in *First European Workshop on Biometrics and Identity Management (BioID)*, ser. Lecture Notes in Computer Science. Springer, 2008, vol. 5372, pp. 181–190.
- [38] A. Czajka, "Database of iris printouts and its application: Development of liveness detection method for iris recognition," in *Int. Conference on Methods and Models in Automation and Robotics (MMAR)*, Aug 2013, pp. 28–33.
- [39] A. F. Sequeira, J. Murari, and J. S. Cardoso, "MobBIO a multimodal database captured with a handheld device," in *Int. Conference on Computer Vision Theory and Applications (VISAPP)*, 2014, pp. 133–139.
- [40] I. Chingovska, A. Anjos, and S. Marcel, "On the effectiveness of local binary patterns in face anti-spoofing," in *Int. Conference of the Biometrics Special Interest Group (BIOSIG)*, 2012, pp. 1–7.
- [41] N. Erdogmus and S. Marcel, "Spoofing in 2d face recognition with 3d masks and anti-spoofing with kinect," in *IEEE Int. Conference on Biometrics: Theory Applications and Systems (VISAPP)*, 2013, pp. 1–6.
- [42] J. Galbally, S. Marcel, and J. Fierrez, "Image quality assessment for fake biometric detection: Application to iris, fingerprint, and face recognition," *IEEE Trans. Image Process.*, vol. 23, no. 2, pp. 710–724, 2014.
- [43] J. Daugman, *Biometrics: Personal Identification in Networked Society*. Kluwer Academic Publishers, 1999, ch. Recognizing Persons by Their Iris Patterns, pp. 103–121.
- [44] —, "Iris recognition and anti-spoofing countermeasures," in *International Biometrics Conference*, 2004.
- [45] E. Lee, K. Park, and J. Kim., "Fake iris detection by using purkinje image," in *Advances in Biometrics*, ser. Lecture Notes in Computer Science. Springer, 2005, vol. 3832, pp. 397–403.
- [46] A. Pacut and A. Czajka, "7," in *Annual IEEE International Carnahan Conference Security Technology*, 2006, pp. 122–129.
- [47] M. Kanematsu, H. Takano, and K. Nakamura, "Highly reliable liveness detection method for iris recognition," in *Annual Conference SICE*, 2007, pp. 361–364.
- [48] Z. Wei, X. Qiu, Z. Sun, and T. Tan, "Counterfeit iris detection based on texture analysis," in *Int. Conference on Pattern Recognition (ICPR)*, 2008, pp. 1–4.
- [49] N. Kohli, D. Yadav, M. Vatsa, and R. Singh, "Revisiting iris recognition with color cosmetic contact lenses," in *IAPR Int. Conference on Biometrics (ICB)*, 2013, pp. 1–7.
- [50] J. Doyle, K. Bowyer, and P. Flynn, "Variation in accuracy of textured contact lens detection based on sensor and lens pattern," in *IEEE Int. Conference on Biometrics: Theory Applications and Systems (VISAPP)*, 2013, pp. 1–7.
- [51] X. Huang, C. Ti, Q. zhen Hou, A. Tokuta, and R. Yang, "An experimental study of pupil constriction for liveness detection," in *IEEE Workshop on Applications of Computer Vision (WACV)*, 2013, pp. 252–258.
- [52] T. Kathikeyan and B. Sabarigiri, "Countermeasures against iris spoofing and liveness detection using electroencephalogram (eeg)," in *Int. Conference on Computing, Communication and Applications (ICCA)*, 2012, pp. 1–5.
- [53] J. Galbally, J. Ortiz-Lopez, J. Fierrez, and J. Ortega-Garcia, "Iris liveness detection based on quality related features," in *IAPR Int. Conference on Biometrics (ICB)*, 2012, pp. 271–276.
- [54] P. Pudil, J. Novovičová, and J. Kittler, "Floating search methods in feature selection," *Pattern Recognition Letters*, vol. 15, no. 11, pp. 1119–1125, 1994.
- [55] J. Fierrez-Aguilar, J. Ortega-garcia, D. Torre-toledano, and J. Gonzalez-rodriguez, "Biosec baseline corpus: A multimodal biometric database," *Pattern Recognition*, vol. 40, pp. 1389–1392, 2007.
- [56] A. F. Sequeira, J. Murari, and J. S. Cardoso, "Iris liveness detection methods in mobile applications," in *Int. Conference on Computer Vision Theory and Applications (VISAPP)*, 2014, pp. 22–33.
- [57] —, "Iris liveness detection methods in the mobile biometrics scenario," in *International Joint Conference on Neural Network (IJCNN)*, 2014, pp. 1–6.
- [58] J. C. Monteiro, A. F. Sequeira, H. P. Oliveira, and J. S. Cardoso, "Robust iris localisation in challenging scenarios," in *CCIS Communications in Computer and Information Science*. Springer-Verlag, 2004.

- [59] J. Doyle and K. W. Bowyer, "Notre dame image dataset for contact lens detection in iris recognition," 2014, last access on June 2014. [Online]. Available: http://www3.nd.edu/~cvrl/CVRL/Data_Sets.html
- [60] V. Ojansivu and J. Heikkilä, "Blur insensitive texture classification using local phase quantization," in *Int. Conference on Image and Signal Processing (ICISP)*, 2008, pp. 236–243.
- [61] Z. Z. L. Zhang and H. Li., "Binary gabor pattern: an efficient and robust descriptor for texture classification," in *IEEE Int. Conference on Image Processing (ICIP)*, 2012, pp. 81–84.
- [62] T. Ojala, M. Pietikainen, and T. Maenpää, "Multiresolution gray-scale and rotation invariant texture classification with local binary patterns," *IEEE Trans. Pattern Anal. Mach. Intell.*, vol. 24, no. 7, pp. 971–987, 2002.
- [63] Z. Sun, H. Zhang, T. Tan, and J. Wang, "Iris image classification based on hierarchical visual codebook," *IEEE Trans. Pattern Anal. Mach. Intell.*, vol. 36, no. 6, pp. 1120–1133, 2014.
- [64] W. Robson Schwartz, A. Rocha, and H. Pedrini, "Face spoofing detection through partial least squares and low-level descriptors," in *IEEE Int. Joint Conference on Biometrics (IJCB)*, 2011, pp. 1–8.
- [65] J. Määttä, A. Hadid, and M. Pietikäinen, "Face spoofing detection from single images using micro-texture analysis," in *IEEE Int. Joint Conference on Biometrics (IJCB)*, 2011, pp. 1–7.
- [66] A. Anjos and S. Marcel, "Counter-measures to photo attacks in face recognition: a public database and a baseline," in *International Joint Conference on Biometrics 2011*, 2011, pp. 1–7.
- [67] T.-W. Lee, G.-H. Ju, H.-S. Liu, and Y.-S. Wu, "Liveness detection using frequency entropy of image sequences," in *IEEE Int. Conference on Acoustics, Speech, and Signal Processing (ICASSP)*, 2013, pp. 2367–2370.
- [68] N. Erdogmus and S. Marcel, "Spoofing 2D face recognition systems with 3D masks," in *Int. Conference of the Biometrics Special Interest Group (BIOSIG)*, 2013, pp. 1–8.
- [69] W. Zhang, S. Shan, W. Gao, X. Chen, and H. Zhang, "Local gabor binary pattern histogram sequence (lgbphs): a novel non-statistical model for face representation and recognition," in *IEEE Int. Conference on Computer Vision (ICCV)*, vol. 1, 2005, pp. 786–791.
- [70] L. Wiskott, J.-M. Fellous, N. Kuiger, and C. Von der Malsburg, "Face recognition by elastic bunch graph matching," *IEEE Trans. Pattern Anal. Mach. Intell.*, vol. 19, no. 7, pp. 775–779, 1997.
- [71] M. Günther, D. Haufe, and R. P. Würtz, "Face recognition with disparity corrected gabor phase differences," in *Int. Conference on Artificial Neural Networks and Machine Learning (ICANN)*, 2012, pp. 411–418.
- [72] N. Kose and J.-L. Dugelay, "On the vulnerability of face recognition systems to spoofing mask attacks," in *IEEE Int. Conference on Acoustics, Speech, and Signal Processing (ICASSP)*, 2013, pp. 2357–2361.
- [73] —, "Countermeasure for the protection of face recognition systems against mask attacks," in *IEEE Int. Conference and Workshops on Automatic Face and Gesture Recognition (FG)*, 2013, pp. 1–6.
- [74] X. Tan, Y. Li, J. Liu, and L. Jiang, "Face liveness detection from a single image with sparse low rank bilinear discriminative model," in *European Conference on Computer Vision (ECCV)*, 2010, pp. 504–517.
- [75] N. Kose and J.-L. Dugelay, "Reflectance analysis based countermeasure technique to detect face mask attacks," in *Int. Conference on Digital Signal Processing (DSP)*, 2013, pp. 1–6.
- [76] T. de Freitas Pereira, A. Anjos, J. De Martino, and S. Marcel, "Can face anti-spoofing countermeasures work in a real world scenario?" in *IAPR Int. Conference on Biometrics (ICB)*, 2013, pp. 1–8.
- [77] T. Freitas Pereira, J. Komulainen, A. Anjos, J. De Martino, A. Hadid, M. Pietikainen, and S. Marcel, "Face liveness detection using dynamic texture," *EURASIP Journal on Image and Video Processing*, vol. 2014, no. 1, p. 2, 2014.
- [78] J. Galbally, F. Alonso-Fernandez, J. Fierrez, and J. Ortega-Garcia, "Fingerprint liveness detection based on quality measures," in *Int. Conference on Biometrics, Identity and Security (BIDS)*, 2009, pp. 1–8.
- [79] —, "A high performance fingerprint liveness detection method based on quality related features," *Future Generation Computer Systems*, vol. 28, no. 1, pp. 311–321, 2012.
- [80] L. Ghiani, G. Marcialis, and F. Roli, "Fingerprint liveness detection by local phase quantization," in *Int. Conference on Pattern Recognition (ICPR)*, 2012, pp. 537–540.
- [81] D. Gagnaniello, G. Poggi, C. Sansone, and L. Verdoliva, "Fingerprint liveness detection based on weber local image descriptor," in *IEEE Workshop on Biometric Measurements and Systems for Security and Medical Applications*, 2013, pp. 46–50.
- [82] V. Ojansivu, E. Rahtu, and J. Heikkilä, "Rotation invariant local phase quantization for blur insensitive texture analysis," in *Int. Conference on Pattern Recognition (ICPR)*, 2008, pp. 1–4.
- [83] X. Jia, X. Yang, Y. Zang, N. Zhang, R. Dai, J. Tian, and J. Zhao, "Multi-scale block local ternary patterns for fingerprints vitality detection," in *IAPR Int. Conference on Biometrics (ICB)*, 2013, pp. 1–6.
- [84] L. Ghiani, A. Hadid, G. Marcialis, and F. Roli, "Fingerprint liveness detection using binarized statistical image features," in *IEEE Int. Conference on Biometrics: Theory Applications and Systems (VISAPP)*, 2013, pp. 1–6.
- [85] J. Kannala and E. Rahtu, "Bsf: Binarized statistical image features," in *Int. Conference on Pattern Recognition (ICPR)*, 2012, pp. 1363–1366.
- [86] A. Hyvriinen, J. Hurri, and P. O. Hoyer, *Natural Image Statistics: A Probabilistic Approach to Early Computational Vision*, 1st ed. Springer Publishing Company, Incorporated, 2009.
- [87] W. S. Geisler and D. G. Albrecht, "Cortical neurons: Isolation of contrast gain control," *Vision Research*, vol. 32, no. 8, pp. 1409–1410, 1992.
- [88] P. Viola and M. Jones, "Robust real-time object detection," *Int. Journal of Computer Vision*, vol. 57, no. 2, pp. 137–154, 2001.
- [89] A. A. Ross, K. Nandakumar, and A. K. Jain, "Score level fusion," in *Handbook of Multibiometrics*, ser. International Series on Biometrics. Springer US, 2006, vol. 6, pp. 91–142.
- [90] J. Bergstra, D. Tamins, and N. Pinto, "Hyperparameter optimization for convolutional vision architecture," 2013. [Online]. Available: <https://github.com/hyperopt/hyperopt-convnnet>
- [91] J. Bergstra, O. Breuleux, F. Bastien, P. Lamblin, R. Pascanu, G. Desjardins, J. Turian, D. Warde-Farley, and Y. Bengio, "Theano: a CPU and GPU math expression compiler," in *The Python for Scientific Computing Conference (SciPy)*, 2010.
- [92] G. Chiachia, "Random convolutional networks for iris, face, and fingerprint spoofing attacks," 2014. [Online]. Available: <https://bitbucket.org/chiachia/simple-hp>